Acta Oceanol. Sin., 2023, Vol. 42, No. 8, P. 77–86
https://doi.org/10.1007/s13131-023-2212-8
http://www.aosocean.com
E-mail: ocean2@hyxb.org.cn

Spatial distribution and export of nutrients and metal elements in the subterranean estuary of Daya Bay

Zhaoxi Liu[1†], Mingchen Ge[1†], Qianqian Wang[2*], Xuejing Wang[3], Kai Xiao[2], Gang Li[2], Hailong Li[1, 2]

[1] School of Water Resources and Environmental Science, China University of Geosciences, Beijing 100083, China

[2] School of Environmental Science and Engineering, Southern University of Science and Technology, Shenzhen 518055, China

[3] Institute of Surface-Earth System Science, School of Earth System Science, Tianjin University, Tianjin 300072, China

Received 5 March 2023; accepted 11 May 2023

Abstract

Subterranean estuaries (STE) are important seawater-groundwater mixing zones with complex biogeochemical processes, which play a vital role in the migration and transformation of dissolved materials. In this study, we first investigated the spatial distributions of dissolved inorganic nitrogen (DIN), dissolved inorganic phosphorous (DIP), dissolved inorganic silicon (DSi) and metal elements (As, Ba, Cr, Cu, Fe, Mn, Ni, Pb, and Zn) in STE including upper intertidal, seepage face and subtidal zones. We then estimated submarine groundwater discharge (SGD) and associated nutrient and metal element fluxes. From the generalized Darcy's law method, SGD was estimated to be 30.13 cm/d, which was about 7 times larger than the inflow (4.16 cm/d). The nutrient and metal fluxes from SGD were estimated to be (5.33 ± 4.99) mmol/(m^2·d) for DIN, (0.22 ± 0.03) mmol/(m^2·d) for DIP, (16.20 ± 2.05) mmol/(m^2·d) for DSi, (1 325.06 ± 99.10) μmol/(m^2·d) for Fe, (143.41 ± 25.13) μmol/(m^2·d) for Mn, (304.06 ± 81.07) μmol/(m^2·d) for Zn, (140.21 ± 13.33) μmol/(m^2·d) for Cu, (84.49 ± 2.94) μmol/(m^2·d) for Pb, (37.38 ± 5.51) μmol/(m^2·d) for Ba, (27.88 ± 3.89) μmol/(m^2·d) for Cr, (10.10 ± 6.33) μmol/(m^2·d) for Ni, and (6.25 ± 3.45) μmol/(m^2·d) for As. The nutrient and metal fluxes from SGD were relatively higher than those from the inflow, suggesting that nearshore groundwater acted as the sources of nutrients and metal elements discharging into the sea. The environmental potential pollution of coastal seawater was evaluated by pollution factor index (P_i), comprehensive water quality index (CWQI), and ecological risk index (ERI). Pb mainly caused potential danger of nearshore environment with considerable contamination (P_i = 5.78 ± 0.19), heavy pollution (CWQI = 4.09) and high ecological risk (ERI = 18.00). This study contributed to better understanding the behavior of nutrients and metal elements and improving the sustainable management of STE under the pressure of anthropogenic activities and climate change.

Key words: subterranean estuaries, submarine groundwater discharge, nutrients, metal elements, pollution assessment, Daya Bay

Citation: Liu Zhaoxi, Ge Mingchen, Wang Qianqian, Wang Xuejing, Xiao Kai, Li Gang, Li Hailong. 2023. Spatial distribution and export of nutrients and metal elements in the subterranean estuary of Daya Bay. Acta Oceanologica Sinica, 42(8): 77–86, doi: 10.1007/s13131-023-2212-8

1 Introduction

Subterranean estuaries, as reactive mixing zones of terrestrial groundwater and recirculated seawater, can act as both geochemical sources and sinks to the coastal ocean (Moore, 1999; Santos et al., 2009). Owing to relevant physical and biogeochemical processes, water flow processes and the migration and transformation of dissolved materials are complex and variable in subterranean estuaries (Li et al., 1999; Wang et al., 2021a; Chen et al., 2022). Submarine groundwater discharge (SGD) is defined as any flow of water on continental margins from the seabed to the coastal ocean (Burnett et al., 2003; Moore, 2003). SGD is an important hydrological process in subterranean estuaries (Burnett et al., 2006). A series of investigations have demonstrated that SGD is a vital transport pathway that delivers terrestrial dissolved nutrients, carbon, and metal elements to the ocean (Garcia-Solsona et al., 2010; Chen et al., 2021; Xu et al., 2022). Therefore, quantification of SGD and associated terrestrial materials in subterranean estuaries is crucial for studying the geochemical cycles of elements in the ocean.

The chemical components of groundwater in subterranean estuaries, especially the pH and salinity, vary both spatially and temporally (Liu et al., 2018b; Sun et al., 2015). The distribution of metal elements and nutrients in subterranean estuaries is mainly related to terrestrial hydraulic gradients, redox reactions, dissolution, precipitation, desorption, adsorption, and biogeochemical processes (including mineralization, nitrification, and denitrification) (Santos et al., 2008). The production and removal of dissolved organic carbon were determined by heterotrophic microorganisms from the seepage face at a depth of 0–20 cm (Jiang et al., 2020). Recent investigations have indicated that the migra-

Foundation item: The National Key R&D Program of China under contract No. 2021YFC3200501; the National Natural Science Foundation of China under contract Nos 42107055 and 42130703; the Fund of Shenzhen Science and Technology Innovation Committee under contract No. 20200925174525002.

*Corresponding author, E-mail: wangqq@sustech.edu.cn

†These authors contributed equally to this work.

tion and transformation of nitrogen in intertidal groundwater are influenced by SGD and microbial activities (Xiao et al., 2018). Many primary producers and marine organisms may be limited by the high concentration of dissolved Fe (Sanders et al., 2012). Furthermore, Fe and Mn have been considered alternative electron acceptors in the bacterial oxidation of organic matter (Garcia-Orellana et al., 2014).

The generalized Darcy's law method has been widely used to quantify SGD in subterranean estuaries (Ma et al., 2015; Li et al., 2018). This method, based on the vertical hydraulic gradient and vertical permeability coefficient, can directly and conveniently obtain the water exchange fluxes between groundwater and seawater (Liu et al., 2018a). The subtidal zone is an important part of a subterranean estuary. However, when the terrestrial material fluxes derived by SGD are calculated, the part from the subtidal zone should also be taken into account, which has been neglected in many studies (Shum and Sundby, 1996; Wang et al., 2017). Significant fluxes of terrestrial materials from SGD may affect coastal ecosystems and even lead to coastal environmental problems, such as eutrophication, water hypoxia, and the death of marine organisms (Rodellas et al., 2014; Wang et al., 2021b; Zhong et al., 2022).

Metal element pollution in subterranean estuaries has attracted increasing attention owing to intensive anthropogenic activities, including increasing population growth and industrial expansion (Syvitski et al., 2005; Babu et al., 2021). Metal elements are considered vital indicators for evaluating the health conditions of both land and marine ecosystems (Hu et al., 2013; Luo et al., 2022). The accumulation of metal elements usually occurs in marine organisms because of the high metal element concentrations in coastal waters, which may affect human health through the food chain and skin contact (Liu et al., 2018b). Multiple indices, including the pollution factor index (P_i), comprehensive water quality index (CWQI), potential ecological risk index (ERI), metal pollution index (MPI), and single-factor contamination index (SFCI) were used to assess the pollution level through the concentration of metal elements in groundwater. Previous studies have focused on metal elements in seawater and sediments rather than those in coastal groundwater (Abou Zakhem and Hafez, 2015; Cao et al., 2015).

This study aimed to investigate the distributions of metal elements (Fe, Zn, Pb, Mn, Cu, Ba, Cr, As, and Ni) and nutrients (dissolved inorganic nitrogen, DIN; dissolved inorganic phosphorus, DIP; and dissolved inorganic silicon, DSi) in both the intertidal and subtidal zones of subterranean estuaries and to discuss the potential migration mechanism of metal elements and nutrients through principal component analysis and correlation analysis. SGD was quantified based on the generalized Darcy's law method, and SGD-associated metal element and nutrient fluxes were estimated. Finally, indicators (P_i, CWQI, and ERI) were used to assess the pollution conditions of groundwater in the subterranean estuary.

2 Materials and methods

2.1 *Study site*

The study site is a coastal sandy aquifer in the Daya Bay (22.45°–22.83°N, 114.50°–114.89°E), a semi-enclosed subtropical embayment located on the eastern coast of Guangdong Province, China (Fig. 1). The Daya Bay covers an area of ~550 km^2 with a depth of 6–16 m and an average of 10 m. Tidal currents in the region are dominated by semidiurnal irregular tides with a maximum tidal range of 2.5 m. The climate conditions in the study region were controlled by the subtropical monsoon system. The average annual temperature is 22℃, and the average annual precipitation is 1 700 mm, with 80% of the rainfall occurring from April to September. No large rivers flow into the bay, but there are several seasonal rivers. The Dan'ao River, which accounts for 70% runoff volume, is the largest among the seasonal rivers, with an average flux of 3.14×10^5 m^3/d. In recent decades, owing to rapid economic growth and urban development, the Daya Bay with its surrounding area, which is a key economic development zone in

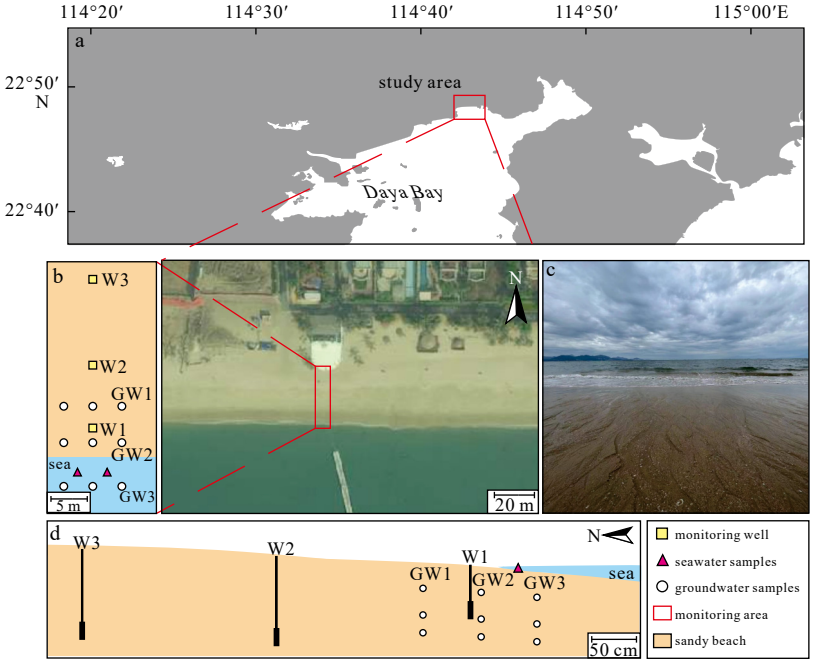

Fig. 1. Location information of the study site: a. Daya Bay; b. sampling area and the spatial distributions of monitoring wells, as well as the groundwater and seawater samplings; c. seepage face zone; d. spatial distributions of monitoring wells (rectangles) including LTC-Diver and sampling points (dots) along the transect from intertidal zone to subtidal zone.

China, has been occupied by shellfish, various industries, and nuclear power plants.

2.2 *Monitoring and sampling collection*

Field campaigns were conducted on a typical sandy beach during spring. Along the transect, three monitoring wells (W1–W3) were set up using PVC tubes and pressure sensors (LTC-Diver, Solinst, Canada). Groundwater level, conductivity, and temperature were monitored by an LTC-Diver installed 0.6 m below the surfaces in W1 and 1.0 m below the surfaces in W2 and W3. The observation period of the monitoring wells in the intertidal zone was from May 19 to 30, 2022. The surface elevations and relative distances of all observed wells were measured with the Real-Time Kinematic positioning technology. Vertical hydraulic conductivity (K_v) was obtained using the falling-head method (Li et al., 2010).

The distribution of the sampling stations is shown in Fig. 1. Groundwater samples (n = 27) were collected in the upper intertidal, seepage face, and subtidal zones at three depths (i.e., 0.3 m, 0.6 m, and 0.8 m) using a stainless steel PushPoint^{TM} groundwater sampler. Two seawater samples were collected from the corresponding positions. In addition, the pH and salinity were measured *in situ* using a calibrated multi-parameter probe (HI 9829, Hanan Instrument, Italy).

All water samples were filtered through 0.45 μm cellulose acetate membranes and then placed into polyethylene bottles stored in a refrigerator (4℃) until laboratory measurement. Nutrient samples for DIN, DIP, and DSi were determined using a spectrophotometer (DR/5 000, American Hach Company) at the Guangdong Provincial Key Laboratory of Soil and Groundwater Pollution Control (China). DIN is the sum of NH_4^+ and NO_x^- ($NO_x^- = NO_3^- + NO_2^-$). Analytical errors were lower than 3% for NO_3^-, 8% for NO_2^-, 10% for NH_4^+, 5% for DIP, and 5% for DSi (Wang et al., 2020). The metal element samples were added HNO_3 to adjust the pH to <2 before storage in a refrigerator. The concentrations of As, Ba, Cr, Cu, Fe, Mn, Ni, Pb, and Zn were analyzed by Inductively Coupled Plasma-Mass Spectrometry (ICP-MS, Thermo Fisher, Germany). Analytical precisions for As, Ba, Cr, Cu, Fe, Mn, Ni, Pb and Zn were 1%, 7%, 3%, 4%, 12%, 6%, 2%, 4%, and 2%, respectively.

2.3 *Seawater-groundwater exchange and flux estimations*

The "single-well method" based on the generalized Darcy's law was used to calculate the vertical flow exchange rate. Vertical groundwater-seawater exchange rate was estimated during the neap-spring tides following the "single-well method" (Ma et al., 2015; Qu et al., 2017):

$$q_i \approx -\delta K_v \left[\frac{h_{sea} - h_w}{\Delta L} + \frac{\varepsilon\,(c_{GW} + c_{SW})}{2}\right], \tag{1}$$

$$J_i \approx -\delta \left[\frac{h_{sea} - h_w}{\Delta L} + \frac{\varepsilon\,(c_{GW} + c_{SW})}{2}\right], \tag{2}$$

where q_i is the groundwater-seawater exchange rate [LT^{-1}]; J_i is the generalized vertical hydraulic gradient [dimensionless]; K_v is the vertical hydraulic conductivity [LT^{-1}]; h_{sea} is the freshwater-equivalent hydraulic head of the tidal level [L]; h_w is the freshwater-equivalent hydraulic head [L] of the observed well; ΔL is the depth of the LTC-Diver when the tide exceeds the surface [L]; c_{GW} and c_{SW} are the observed salinities of groundwater and seawater [ML^{-3}]; salinity is corrected by the conductivity and temperature data; ε is a constant (7.143×10^{-4} m^3/kg); δ is the ratio of the dynamic viscosity of freshwater to saltwater [dimensionless].

Outflow rate (q_{out}) and inflow rate (q_{in}) at each well can be calculated by Eqs (3) and (4). SGD [LT^{-1}] and inflow [LT^{-1}] were defined as the average outflow and inflow rates along the transect in the subterranean estuary. Dissolved material (e.g., nutrients and metal elements) fluxes in subterranean estuaries from SGD can be calculated by the product of average outflow rate (SGD) and the average concentrations of nutrients or metal elements in shallow groundwater. Similarly, nutrient and metal element fluxes from inflow can also be obtained by the product of average inflow rate and the average contents of nutrients or metal elements in seawater.

$$q_{out} = \frac{1}{t_e - t_0}\int_{t_0}^{t_e} \max\{0, q_i(t)\}\mathrm{d}t, \tag{3}$$

$$q_{in} = \frac{1}{t_e - t_0}\int_{t_0}^{t_e} \max\{0, -q_i(t)\}\mathrm{d}t, \tag{4}$$

where q_{out} ($q_i > 0$) and q_{in} ($q_i < 0$) are the outflow and inflow rates, respectively [LT^{-1}]; t_e and t_0 are the end and initial time for the calculated period, respectively.

2.4 *Pollution and ecological risk assessment methods for metal elements*

In this study, the P_i, CWQI, and ERI were chosen to estimate pollution and ecological risk. The P_i was used to evaluate the individual pollution degrees of different metal elements in salt water using the following equation (Hakanson, 1980):

$$P_i = \frac{c_i}{c_b}, \tag{5}$$

where c_i and c_b are the different metal element (i) concentrations of groundwater in the subterranean estuary and its corresponding background concentration, respectively [ML^{-3}], c_b uses the grade three seawater quality standard (GB 3097–1997) for salt water.

Salt water can be divided into four classes based on P_i values. P_i<1, 1≤P_i<3, 3≤P_i<6, 6≤P_i can be considered low contamination, moderate contamination, considerable contamination, and very high contamination, respectively.

The CWQI has been widely used to determine the total pollution degree of seven metal elements in salt water (Sun et al., 2020). CWQI values were calculated using the following equations:

$$\mathrm{CWQI} = \sqrt{\frac{(\max P_i)^2 + (\mathrm{ave}\ P_i)^2}{2}}, \tag{6}$$

where $\max\ P_i$ [-] and ave P_i [-] are the maximum and average P_i values of the metal elements respectively.

Salt water can also be categorized into four grades based on the CWQI value in the following order: negligible pollution (CWQI≤1), slight pollution (1 < CWQI≤2), medium pollution (2 < CWQI≤3), and heavy pollution (CWQI > 3).

ERI was widely used to estimate the potential overall ecological risk of metal elements in the coastal waters. The ERI values of the seven metal elements can be expressed using the following formula:

$$\mathrm{ERI} = \sum_{i}^{n} \left(T_r^i \times \frac{c_i}{\mathrm{PNEC}_i} \right) / \sum_{i}^{n} T_r^i, \tag{7}$$

where T_r^i [-] is the potential ecological risk coefficient and the toxic-response factor of metal element i. The toxic response factors (T_r^i) for Zn, Cr, Cu, Ni, Pb, As, and Cd are 1, 2, 5, 5, 5, 10, and 30, respectively. PNEC_i [ML^{-3}] is the predicted no-effect concentration, which is calculated as the safety factor 5 divided by the US EPA (U.S. Environmental Protection Agency) chronic criterion continuous concentration values. The PNEC_i values for Zn, Cr, Cu, Ni, Pb, As, and Cd were 16.20, 10.00, 0.62, 1.64, 1.12, 7.20, and 1.58, respectively.

Saltwater can be divided into five classes based on the ERI value: no risk (ERI ⩽ 1), low risk (1 < ERI ⩽ 5), moderate risk (5 < ERI ⩽ 10), considerable risk (10 < ERI ⩽ 15), and high risk (ERI > 15).

3 Results

3.1 *Hydrologic dynamic and physicochemical characteristics*

The groundwater level at the observed wells (W1–W3) fluctuated periodically with tides flooding the surface. The tide level ranged from –1.17 m to 1.33 m, with the maximum tidal range of 2.50 m. According to the Fig. 2, water table decreasing from W3 to W1 during low tide, the groundwater discharge was dominate clearly. There was a neap tide during May 25 to May 27 with lower tide levels compared with other periods. W3 was located at the upper intertidal zone close to the supratidal zone with a relatively higher surface level and groundwater level. During a neap tide (May 25 to May 27), lower tide levels had little influence on the water table at W3. The K_v measured using the falling-head method were 3.35×10^{-5} m/s and 2.14×10^{-5} m/s for W1 and W2, respectively. The generalized vertical hydraulic gradient varied from –0.28 to 0.56 for W1 and from –0.07 to 0.91 for W2, respectively. In the high tide and low tide periods, the generalized vertical hydraulic gradient was generally relatively large compared with other periods, which indicated that seawater-groundwater exchange was stronger.

Figure 3 shows the spatial distribution of the physicochemical parameters in the groundwater. It is clear that the pH in groundwater decreased from land to sea, and the pH in shallow groundwater (7.78, n = 9) was slightly higher than that in deep

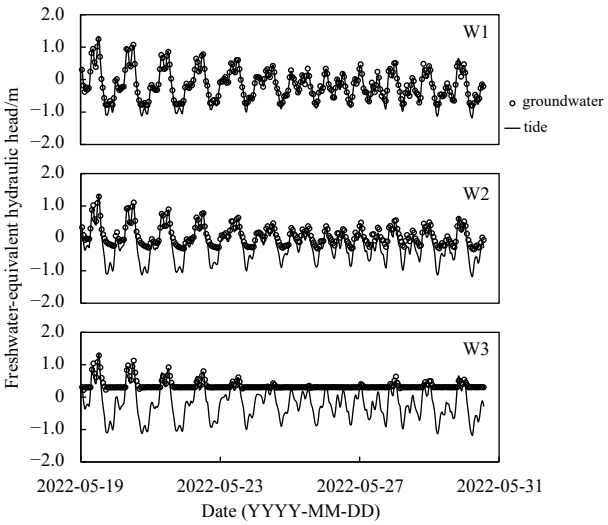

Fig. 2. Time series of groundwater levels and tide levels from May 19 to 30, 2022 at W1, W2, and W3.

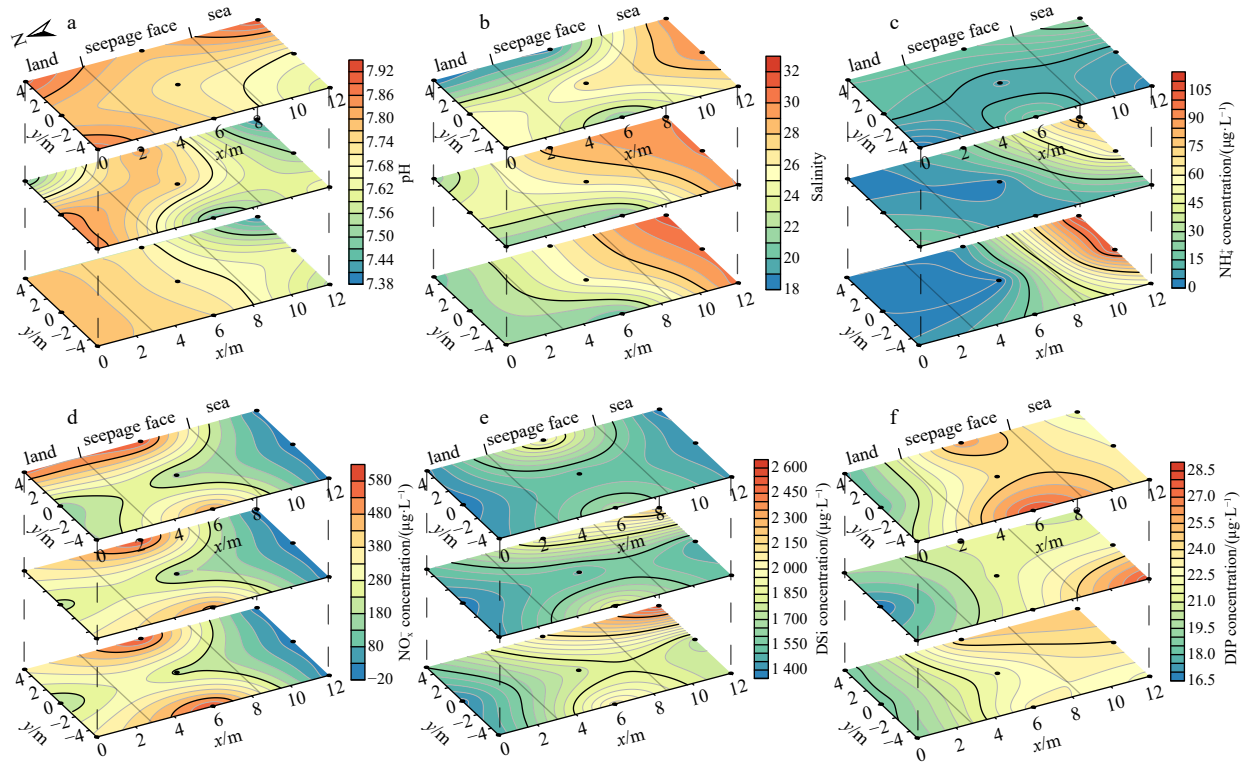

Fig. 3. Spatial distributions of physicochemical parameters and nutrients, including pH (a), salinity (b), NH_4^+ (c), NO_x^- ($NO_x^- = NO_3^- + NO_2^-$) (d), dissolved inorganic silicon (DSi) (e), and dissolved inorganic phosphorous (DIP) (f). The black dots mean the sampling points of groundwater.

groundwater (7.68, n = 9). The salinity varied from 18.4 to 31.5, which gradually increased from land to sea with the highest pH value in the deep subtidal zone and a minimum in the shallow seepage face and the upper intertidal zones. The salinity increased with depth in the subtidal zone: shallow layer (28.6, n = 3) < middle layer (30.1, n = 3) < deep layer (30.8, n = 3), which was opposite in the upper intertidal zone: shallow layer (23.1, n = 3) > middle layer (22.5, n = 3) > deep layer (21.4, n = 3).

3.2 *Spatial distributions of nutrient concentrations*

The concentration distributions of nutrients for the groundwater samples are shown in Fig. 3. The average concentration of NH_4^+ in seawater was 27.12 μg/L (n = 2). The concentrations of NH_4^+ in groundwater ranged from 0.00 μg/L to 108.01 μg/L with an average value of 23.16 μg/L (n = 27). The average NH_4^+ concentrations of groundwater in the upper intertidal, seepage surface, and subtidal zones were 7.30 μg/L, 10.92 μg/L, and 51.25 μg/L, respectively, which gradually increased from the land to the sea (Fig. 3c). In the upper intertidal and seepage surface zones, NH_4^+ concentrations in groundwater decreased with depth, whereas they increased with depth in the subtidal zone. The concentration of NO_x^- in seawater was below the detection limit. The NO_x^- content in groundwater varied from 0.00 μg/L to 598.88 μg/L with an average concentration of 243.73 μg/L (n = 27) (Fig. 3d). The average concentration of NO_x^- in groundwater in the seepage face (434.18 μg/L) and upper intertidal zone (295.58 μg/L) were obviously larger than that in the subtidal zone (1.41 μg/L), which was close to the concentration of NO_x^- in seawater. The seepage face zone, the most active seawater-groundwater mixing zone, showed a relatively high NO_x^- concentration.

The average concentration of DSi in seawater was 853.03 μg/L. The average concentration of DSi among the three zones was 1 658.09 μg/L (n = 27). The concentration of DSi in groundwater in the seepage surface zone was higher than others: seepage face (1 824.42 μg/L, n = 9) > subtidal zone (1 710.53 μg/L, n = 9) > upper intertidal zone (1 438.34 μg/L, n = 9). In addition, the concentration of DSi in the groundwater increased with depth, and a high DSi content area was formed in the deep layer (Fig. 3e). The concentration of DIP in seawater was below the detection limit, while the concentration of DIP in groundwater had a small range of variation, which varied from 16.68 μg/L to 27.86 μg/L with the average concentration of 21.97 μg/L (n = 27) (Fig. 3f). The average DIP concentrations in the seepage face (23.66 μg/L, n = 9) and the subtidal zone (23.54 μg/L, n = 9) were a bit larger than these in the upper intertidal zone (18.69 μg/L, n = 9).

3.3 *Spatial distributions of metal elements*

The concentrations of metal elements in groundwater ranged from 0.15 μg/L to 6.20 μg/L for As, from 13.10 μg/L to 25.65 μg/L for Ba, from 46.00 μg/L to 102.70 μg/L for Zn, from 3.65 μg/L to 5.95 μg/L for Cr, from 25.65 μg/L to 34.05 μg/L for Cu, from 214.65 μg/L to 292.20 μg/L for Fe, from 19.45 μg/L to 55.05 μg/L for Mn, from 53.70 μg/L to 60.90 μg/L for Pb and from 0.85 μg/L to 5.95 μg/L for Ni (Fig. 4), with average concentrations of 243.59 μg/L, 67.80 μg/L, 57.78 μg/L, 29.34 μg/L, 28.71 μg/L, 17.71 μg/L, 4.59 μg/L, 2.03 μg/L, 1.79 μg/L, respectively (n = 27). The average concentrations of Fe, Zn, Pb, Mn, Cu, Ba, Cr, Ni, and As in seawater were 310.73 μg/L, 85.30 μg/L, 58.65 μg/L, 39.20 μg/L, 32.10 μg/L, 14.23 μg/L, 6.00 μg/L, 1.75 μg/L, 1.70 μg/L (n = 2), respectively. The average concentrations of Fe, Zn, Mn, Cu, and Cr in seawater were higher than those in groundwater, whereas the concentrations of As and Ba were the opposite. In addition, the average concentrations of Ni and Pb in groundwater were similar to those in seawater.

The average As concentration of groundwater in the seepage face (1.73 μg/L, n = 9), similar to the seawater (1.70 μg/L), was smaller than that in the upper intertidal zone (1.83 μg/L, n = 9) and subtidal zone (2.51 μg/L, n = 9) (Fig. 4a). While the mean concentration of Ba in groundwater (17.71 μg/L, n = 27) was higher than that in seawater (14.23 μg/L), especially in the seepage surface (20.02 μg/L, n = 9). The Ba content of the groundwater increased with depth (Fig. 4b). Compared with the upper intertidal and subtidal zones, the average Cr concentration in the seepage face (4.96 μg/L, n = 9) was higher and decreased with depth. In addition, a more obvious gradient change in the Cr concentration was observed in the deep layer than in the other layers (Fig. 4c).

The average concentrations of Fe and Cu in seawater (310.73 μg/L, 32.10 μg/L, n = 2) were significantly higher than those in the groundwater (243.59 μg/L, 28.71 μg/L, n = 27). A higher concentration of Fe appeared in the deep layer of the upper intertidal and subtidal zones as well as in the middle layer of the seepage face (Fig. 4e). The Cu in the seepage zone decreased with depth and was larger than that in the upper intertidal zone (Fig. 4d). The concentration of Mn in the groundwater in the upper intertidal (27.25 μg/L, n = 9) and seepage zone (28.56 μg/L, n = 9) was much lower than that of seawater (39.20 μg/L), which was approximately half of that of the groundwater in the subtidal zone (66.29 μg/L, n = 9). Mn increased with depth, particularly in the subtidal zone (Fig. 4f). A clearer gradient distribution of Mn was observed in the deep layer compared with the shallow and middle layers from the land to the sea.

The maximum concentration of Pb (60.90 μg/L) was detected in the shallow seepage face, and the average concentration in the shallow layer (58.04 μg/L, n = 9) was slightly higher than that in the middle layer (57.61 μg/L, n = 9) and deep layer (57.68 μg/L, n = 9). Pb increased with depth in the upper intertidal zone, but decreased with depth in the subtidal zone (Fig. 4h). The average concentration of Ni in the subtidal groundwater (1.78 μg/L, n = 9) was similar to that of seawater (1.75 μg/L). The concentration of Ni in the groundwater was higher in the shallow and deep layers of the seepage face and relatively lower in other zones (Fig. 4g). There is an obvious gradient of Zn in the groundwater, whose concentration decreases from land to sea (Fig. 4i). The average concentration of Zn in groundwater in the subtidal zone is only 57.27 μg/L, which is approximately two-thirds of that in the upper intertidal zone (85.91 μg/L, n = 9).

4 Discussion

4.1 *Controlling mechanism on nutrients and metal elements in different zones*

Principal component analysis (PCA) and Pearson correlation are generally used to analyze the association among physicochemical parameters, metal elements, and nutrients. PCA of the nutrients and metal elements revealed five principal components with F1, F2, F3, F4, and F5 accounting for 28.75%, 19.01%, 13.25%, 11.24%, and 7.21% of the total variance, respectively.

The bi-plot of the two principal components (PCs) indicated that the distribution of groundwater samples among the three zones had clear zoned characteristics (Fig. 5). The F1 axis separated the groundwater samples in the upper tidal zone from those in the subtidal zone, suggesting that the spatial distributions of physicochemical characteristics (e.g., pH and salinity) in subterranean estuaries may influence the distribution of nutrients and metal elements from land to sea (Fig. 5). The F1 was mainly composed of pH, salinity, Cr, Zn, Mn, DIP, $NO_x^-$and NH_4^+. Figure 6

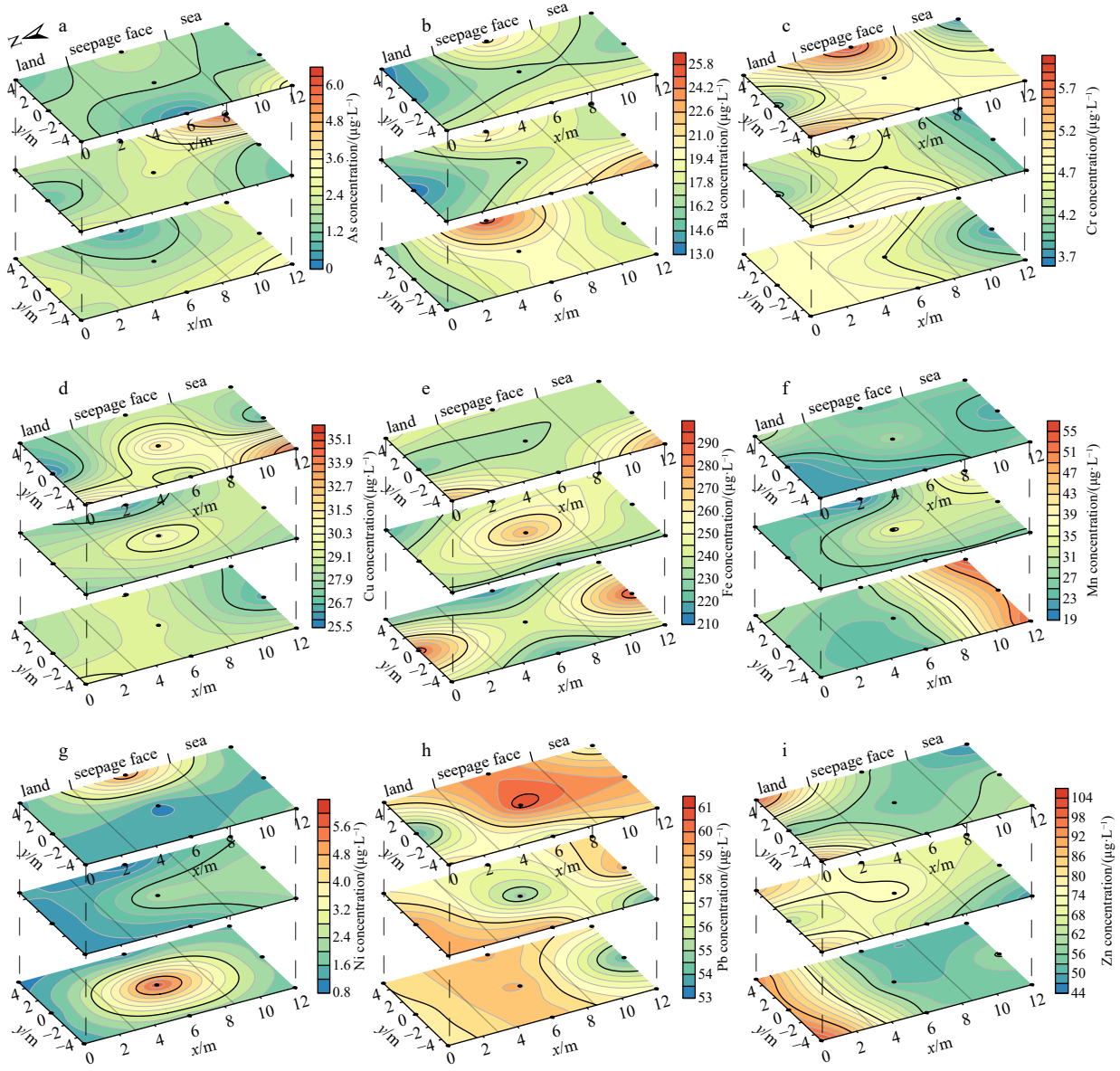

Fig. 4. Spatial distributions of metal elements, including As (a), Ba (b), Cr (c), Cu (d), Fe (e), Mn (f), Ni (g), Pb (h), and Zn (i). The black dots mean the sampling points of groundwater.

showed that pH was negatively correlated with salinity ($p < 0.05$) and strongly negatively correlated with Mn and NH_4^+ ($p < 0.01$). Salinity showed different degrees of negative relationships with Zn ($p < 0.01$), Cr, and NO_x^- ($p < 0.001$). The form of nitrogen was dominated by NH_4^+ in seawater and groundwater of subtidal zone. Because the relatively high microbial content in seawater, particularly in summer, may consume more oxygen and form a relatively reducing environment, denitrification may be predominant in the nitrogen cycle (Xiao et al., 2018). In addition, the oxidation environment decreased with depth, which was conducive to denitrification, especially in the subtidal zone. NO_x^- was mainly derived from terrestrial sources, which may be caused by anthropogenic activities such as domestic wastewater and waste (Dun et al., 2022). In addition to the natural sources of Zn and Cr released from organic matter in sediments or enrichment of carbonate facies (Wang et al., 2016), industrial and agricultural pollution may be considered a more important terrestrial source of Zn and Cr in groundwater (Wen et al., 2019). The concentration of phosphorus in groundwater increases linearly with salinity, suggesting that may be due to the desorption of DIP from the aquifer by seawater intrusion (Price et al., 2006).

The F2 axis separated the groundwater samples in the seepage face zone from the upper intertidal and subtidal zones, indicating that seawater-groundwater exchange may affect the migration and transformation of nutrients and metal elements (including sediment diffusion or mineral dissolution) (Fig. 5). Ni, Ba, DIP, and DSi performed positive loadings in F2 with different degrees (P-Si, $p < 0.05$; Ba-Si, $p < 0.01$; Ba-P, $p < 0.001$) (Fig. 6). The increases in Ni, Ba, DSi, and DIP with depth are mainly derived from the dissolution and desorption of minerals in the sediments (Millward and Liu, 2003; Mayfield et al., 2021). The seawater-groundwater mixing process is stronger in the intertidal zone, which carries nutrients and metals into ocean, especially in seepage face zone (Li et al., 2008). Therefore, the concentrations of Ni, Ba, and DSi are much higher in seepage face zone than those in the upper intertidal and subtidal zones.

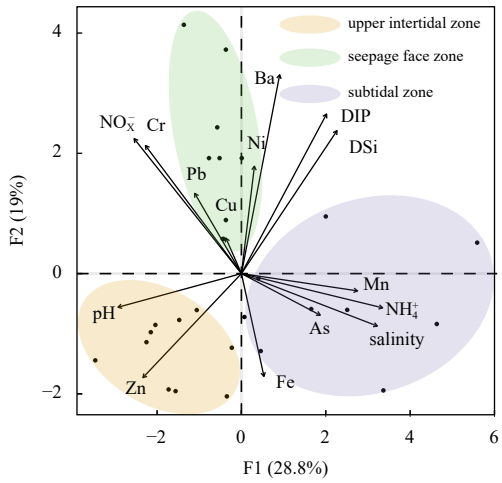

Fig. 5. Principal component analysis (PCA) bi-plot for groundwater samples of upper intertidal (n = 9), seepage face (n = 9) and subtidal zones (n = 9). The samples of three zones have been divided by different color. n means the number of samples.

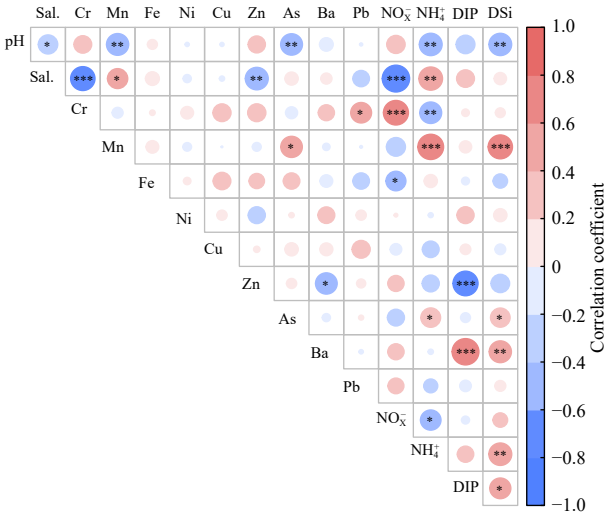

Fig. 6. The Pearson correlations analysis for physicochemical parameters, nutrients, and metal elements of groundwater samples in three zones. Sal. means an abbreviation for salinity.

There was also a positive correlation between As and Mn in the correlation analysis (Fig. 6). Mn in groundwater is mainly produced by the dissolution of Mn-bearing minerals (Guo et al., 2018). The As in groundwater is easily attracted by positively charged substances, such as Fe oxides, Mn oxides, and clay minerals, and adsorbed on these particles. As the reducing conditions in the groundwater were enhanced with depth, As adsorbed on the Fe and Mn oxide particles was released into the groundwater with the dissolution of Mn oxide, and the contents of As and Mn in the groundwater increased (Ho et al., 2019). The positive relationship between Fe and Cu indicated that the distributions of those are affected by the adsorption and dissolution of organic Cu complexes and Fe-oxidized minerals (Fig. 6). Owing to the dissolution of Fe-oxidized minerals, Cu is released from Fe-oxidized minerals (Kim and Kim, 2015). In addition, stronger flow velocity in the intertidal zone also promotes the migration of the organic Cu complex (Montluçon and Sañudo-Wilhelmy, 2001), which may result in a relatively high Cu content on the surface of the seepage face. F5 had a negative Pb loading. A high concentration of Pb appeared in both seawater and groundwater in the surface layer, particularly on the seepage surface. Pb may accumulate in surficial sediments and then migrate through SGD or inflow. Biogeochemical activity enhanced by seawater-groundwater exchange may change the groundwater environment conditions and help Pb release from the particles (Yin et al., 2010).

4.2 *Nutrient and metal element fluxes from SGD*

According to Eq. (1), the seawater-groundwater exchange rate can be conveniently estimated during the spring-neap tide. The average outflow rate (q_{out}) and inflow rate (q_{in}) at W1 in seepage face zone were 15.71 cm/d and 8.12 cm/d calculated by Eqs (3) and (4), respectively. A larger average outflow rate (q_{out}= 44.55 cm/d) and a smaller average inflow rate (q_{in}= 0.20 cm/d) were found at W2 in upper intertidal zone compared with W1. In our study, the average outflow in the upper intertidal zone was larger than that in the seepage face zone. In addition to the heterogeneity of sediments, the large slope of transect (10%) may be another main reason. The average outflow rate (SGD) and average inflow rate were estimated to be 30.13 cm/d and 4.16 cm/d with the net flow rate of 25.97 cm/d. The groundwater discharge rate of the intertidal zone in the Daya Bay subterranean estuary is within the scope of previous studies (Tables 1 and 2).

The average nutrients and metal elements in groundwater in the shallow layer (0.3 m) in the upper intertidal zone, seepage face, and subtidal zone were used as groundwater end-members to estimate the fluxes associated with SGD. The nutrient and metal element fluxes from SGD were estimated (Tables 1 and 2). The nutrients carried by SGD in this study were within the range

Table 1. The nutrient fluxes derived by submarine groundwater discharge (SGD) in the Daya Bay in comparison with other studies

Case studies	SGD/(cm·d^{-1})	Fluxes of nutrients/(mmol·m^{-2}·d^{-1})					Reference
		NO_x^-	NH_4^+	DIN	DIP	DSi	
STE in Daya Bay, China	30.13	5.09	0.24	5.33	0.22	16.20	this study
Daya Bay, China	1.18±0.43	ND	ND	0.285	0.015	2.66	Wang et al. (2018a)
Daya Bay, China	5.3	ND	ND	3.62	0.1	ND	Gao et al. (2018)
Daya Bay, China	28.2–30.9	ND	0.656	ND	0.001 2	1.794	Wang et al. (2017)
Jiaozhou Bay, China	2.12–5.59	ND	ND	4.36	0.04	2.49	Zhang et al. (2020)
Sanya Bay, China	(4.3±2.1)–(7.8±4.1)	ND	ND	8.54	0.1	13.85	Wang et al. (2018b)
Bohai Bay, China	7.3	ND	ND	7.78	0.15	9.26	Wang et al. (2020)
Kakinada Bay, India	17.93	ND	ND	121.21	9.50	199.00	Rengarajan and Sarma (2015)
Masan Bay, Korea	6.1–7.1	ND	ND	1.16–6.01	0.028–0.140	0.74–3.84	Lee et al. (2009)

Note: STE: subterranean estuaries; ND: no data; DIN: dissolved inorganic nitrogen; DIP: dissolved inorganic phosphorous; DSi: dissolved inorganic silicon.

Table 2. The metal fluxes derived by submarine groundwater discharge (SGD) in the Daya Bay in comparison with other studies

Case studies	SGD/(cm·d^{-1})	Fluxes of metal elements/(μmol·m^{-2}·d^{-1})									Reference
		Cr	Mn	Fe	Ni	Cu	Zn	As	Ba	Pb	
STE in Daya Bay, China	30.13	27.88	143.41	1 325.06	10.10	140.21	304.06	6.25	37.38	84.49	this study
Bangdu, Korea	24.38	ND	2.5	270	2.4	0.7	ND	ND	ND	ND	Jeong et al. (2012)
Jiaozhou Bay, China	0.003 6–7.6	11.92	ND	ND	ND	5.87	3.85	0.13	ND	1.59	Qu et al. (2020)
Greater Bay , China	4.57	0.81	ND	ND	0.48	0.7	10.46	2.2	ND	0.03	Luo et al. (2022)
Hailing Island, China	5–10	1.37	ND	70.88	0.2	0.37	24.94	1.88	10.45	0.082	Li et al. (2022)
Bohai Bay	2.00–4.81	1.69–4.63	750.0–1 687.5	125–375	ND	ND	18.75–51.25	ND	ND	ND	Wang et al. (2019)

Note: STE: subterranean estuaries; ND: no data.

of other studies. The metal elements from SGD were larger than those in other studies, especially Fe, Zn, and Pb, which were 1–4 orders of magnitude higher than others (Jeong et al., 2012; Qu et al., 2017; Luo et al., 2022), respectively.

In addition, seawater was chosen as the end-member to analyze the nutrient and metal element fluxes derived by inflow. The nutrient and metal element fluxes from inflow were (0.08 ± 0.01) mmol/(m^2·d) for NH_4^+ and (1.27 ± 0.04) mmol/(m^2·d) for DSi, (230.82 ± 8.15) μmol/(m^2·d) for Fe, (54.59 ± 13.31) μmol/(m^2·d) for Zn, (29.65 ± 14.41) μmol/(m^2·d) for Mn, (21.20 ± 1.29) μmol/(m^2·d) for Cu, (11.79 ± 0.04) μmol/(m^2·d) for Pb, (4.80 ± 0.68) μmol/(m^2·d) for Cr, (4.32 ± 0.31) μmol/(m^2·d) for Ba, (1.26 ± 0.54) μmol/(m^2·d) for Ni, and (0.94 ± 0.00) μmol/(m^2·d) for As (Fig. 7). It was clear that nutrient and metal element fluxes associated with inflow were approximately one order smaller than those derived by SGD. Nearshore groundwater generally acts as a source of nutrients and metal elements that were discharged into the sea.

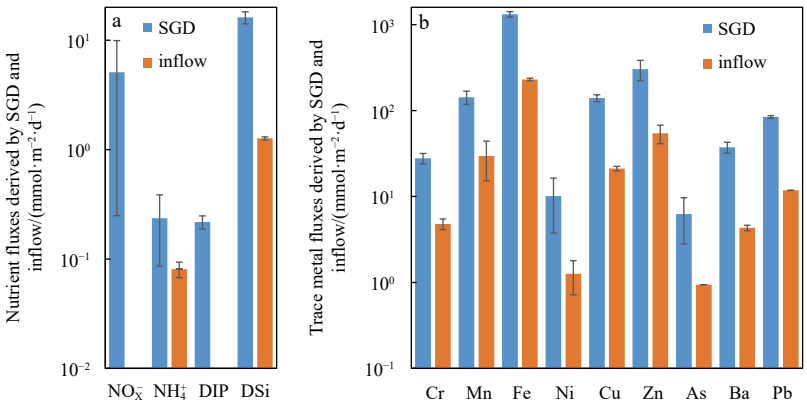

Fig. 7. The nutrient fluxes from submarine groundwater discharge (SGD) and inflow (a); metal element fluxes derived by SGD and inflow (b).

4.3 *Pollution and ecological risk assessment*

The P_i of the six metal elements (Cr, Ni, Zn, Cu, As, and Pb) in groundwater was calculated using Eq. (5) are shown in Fig. 8. Nearshore groundwater in the Daya Bay was mainly polluted by Pb (P_i = 5.78 ± 0.19) with considerable contamination (Class III) rather than other metals (Cr (P_i = 0.46 ± 0.06), Ni (P_i = 0.11 ± 0.11), Cu (P_i = 0.57 ± 0.04), Zn (P_i = 0.68 ± 0.17), and As (P_i = 0.04 ± 0.02)), which were lower in Class I (low contamination). While the CWQI of Daya Bay was estimated by Eq. (6), reaching 4.09, which is larger than the limited standard for heavy pollution. The ERI, estimated using Eq. (7) in this area (ERI = 18.00) was also beyond the high ecological risk (ERI < 15).

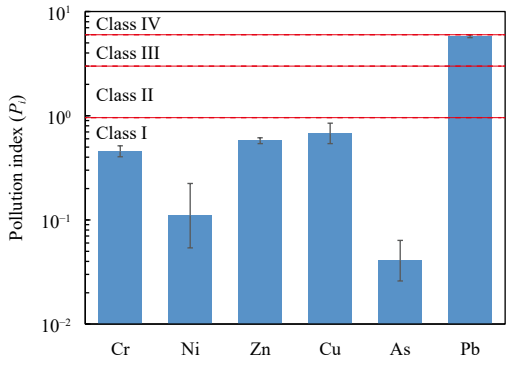

Fig. 8. Pollution factor index of metal elements (Cr, Ni, Zn, Cu, As, and Pb) in the groundwater among three zones.

The results indicated that there was a certain risk of nearshore environmental pollution in the Daya Bay, and the main source of pollution may be Pb. The concentrations of Pb in seawater and groundwater were both higher than the standard for Class III seawater in China; therefore, the potential source of Pb is most likely artificial pollution, which pollutes both seawater and groundwater, such as petrochemical plants (Luo et al., 2022).

5 Conclusions

In this study, we investigated the spatial patterns nutrients and metal elements in the subterranean estuaries (STE) including among upper intertidal, seepage face and subtidal zones of a sandy subterranean estuary. The reasons for spatial distributions of nutrients and metal elements may be related to the seawater-groundwater interactions, sedimentary environments, biogeochemical reactions, and anthropogenic activities. We estimated SGD and associated nutrient and metal element fluxes in the subterranean estuaries. SGD was estimated to be 30.13 cm/d

from the generalized Darcy's law method, which may play an important role in delivering nutrients and metal elements to the Daya Bay. The metal element fluxes and nutrient fluxes from SGD were relatively higher than those from the inflow indicating that nearshore groundwater generally may act as a source of nutrients and metal elements that are discharged into the sea. With large numbers of contaminants discharging to the subterranean estuary via SGD, human health and marine environment may be threatened by the potential pollution. The environmental potential pollutants (Cr, Ni, Zn, Cu, As, and Pb) of coastal seawater were assessed by P_i, CWQI, and ERI. The results of pollution factor index showed that Pb was the main potential danger of nearshore environment with considerable contamination (P_i = 5.78 ± 0.19) compared with others. The six metal elements exhibited heavy pollution (CWQI = 4.09) and high ecological risk (ERI = 18.00) in the subterranean estuaries. This study highlighted the SGD derived nutrient and metal element fluxes had significant implications for the coastal marine system, and it can serve as a scientific reference for the management of subterranean estuaries and further research.

Acknowledgements

This work was supported by the State Environmental Protection Key Laboratory of Integrated Surface Water-Groundwater Pollution Control.

References

Abou Zakhem B, Hafez R. 2015. Heavy metal pollution index for groundwater quality assessment in Damascus Oasis, Syria. Environmental Earth Sciences, 73(10): 6591–6600, doi: 10.1007/s12665-014-3882-5

Babu D S S, Khandekar A, Bhagat C, et al. 2021. Evaluation, effect and utilization of submarine groundwater discharge for coastal population and ecosystem: a special emphasis on Indian coastline. Journal of Environmental Management, 277: 111362, doi: 10.1016/j.jenvman.2020.111362

Burnett W C, Aggarwal P K, Aureli A, et al. 2006. Quantifying submarine groundwater discharge in the coastal zone via multiple methods. Science of the Total Environment, 367(2–3): 498–543

Burnett W C, Bokuniewicz H, Huettel M, et al. 2003. Groundwater and pore water inputs to the coastal zone. Biogeochemistry, 66(1–2): 3–33

Cao Feifei, Kong Linghao, Yang Liyuan, et al. 2015. Geochemical fractions and risk assessment of trace elements in soils around Jiaojia gold mine in Shandong Province, China. Environmental Science and Pollution Research, 22(17): 13496–13505, doi: 10.1007/s11356-015-4618-0

Chen Guangquan, Xu Bochao, Zhao Shibin, et al. 2022. Submarine groundwater discharge and benthic biogeochemical zonation in the Huanghe River Estuary. Acta Oceanologica Sinica, 41(1): 11–20, doi: 10.1007/s13131-021-1882-3

Chen Xiaogang, Du Jinzhou, Yu Xueqing, et al. 2021. Porewater-derived dissolved inorganic carbon and nutrient fluxes in a saltmarsh of the Changjiang River Estuary. Acta Oceanologica Sinica, 40(8): 32–43, doi: 10.1007/s13131-021-1797-z

Dun Yu, Ling Junhong, Wang Rui, et al. 2022. Hydrochemical evolution and nitrogen behaviors in coastal groundwater suffered from seawater intrusion and anthropogenic inputs. Frontiers in Marine Science, 9: 945330, doi: 10.3389/fmars.2022.945330

Gao Jingyan, Wang Xuejing, Zhang Yan, et al. 2018. Estimating submarine groundwater discharge and associated nutrient inputs into Daya Bay during spring using radium isotopes. Water Science and Engineering, 11(2): 120–130, doi: 10.1016/j.wse.2018.06.002

Garcia-Orellana J, Cochran J K, Bokuniewicz H, et al. 2014. Evaluation of ^{224}Ra as a tracer for submarine groundwater discharge in Long Island Sound (NY). Geochimica et Cosmochimica Acta, 141: 314–330, doi: 10.1016/j.gca.2014.05.009

Garcia-Solsona E, Garcia-Orellana J, Masqué P, et al. 2010. An assessment of karstic submarine groundwater and associated nutrient discharge to a Mediterranean coastal area (Balearic Islands, Spain) using radium isotopes. Biogeochemistry, 97(2): 211–229

Guo Xueru, Zuo Rui, Meng Li, et al. 2018. Seasonal and spatial variability of anthropogenic and natural factors influencing groundwater quality based on source apportionment. International Journal of Environmental Research and Public Health, 15(2): 279, doi: 10.3390/ijerph15020279

Hakanson L. 1980. An ecological risk index for aquatic pollution control. A sedimentological approach. Water Research, 14(8): 975–1001, doi: 10.1016/0043-1354(80)90143-8

Ho Peng, Shim M J, Howden S D, et al. 2019. Temporal and spatial distributions of nutrients and trace elements (Ba, Cs, Cr, Fe, Mn, Mo, U, V and Re) in Mississippi coastal waters: influence of hypoxia, submarine groundwater discharge, and episodic events. Continental Shelf Research, 175: 53–69, doi: 10.1016/j.csr.2019.01.013

Hu Bangqi, Li Guogang, Li Jun, et al. 2013. Spatial distribution and ecotoxicological risk assessment of heavy metals in surface sediments of the southern Bohai Bay, China. Environmental Science and Pollution Research, 20(6): 4099–4110, doi: 10.1007/s11356-012-1332-z

Jeong J, Kim G, Han S. 2012. Influence of trace element fluxes from submarine groundwater discharge (SGD) on their inventories in coastal waters off volcanic island, Jeju, Korea. Applied Geochemistry, 27(1): 37–43, doi: 10.1016/j.apgeochem.2011.08.014

Jiang Shan, Zhang Yixue, Jin Jie, et al. 2020. Organic carbon in a seepage face of a subterranean estuary: turnover and microbial interrelations. Science of the Total Environment, 725: 138220, doi: 10.1016/j.scitotenv.2020.138220

Kim I, Kim G. 2015. Role of colloids in the discharge of trace elements and rare earth elements from coastal groundwater to the ocean. Marine Chemistry, 176: 126–132, doi: 10.1016/j.marchem.2015.08.009

Lee Y W, Hwang D W, Kim G, et al. 2009. Nutrient inputs from submarine groundwater discharge (SGD) in Masan Bay, an embayment surrounded by heavily industrialized cities, Korea. Science of the Total Environment, 407(9): 3181–3188, doi: 10.1016/j.scitotenv.2008.04.013

Li L, Barry D A, Stagnitti F, et al. 1999. Submarine groundwater discharge and associated chemical input to a coastal sea. Water Resources Research, 35(11): 3253–3259, doi: 10.1029/1999WR900189

Li Hailong, Boufadel M C, Weaver J W. 2008. Tide-induced seawater–groundwater circulation in shallow beach aquifers. Journal of Hydrology, 352(1–2): 211–224

Li Gang, Li Hailong, Wang Xuejing, et al. 2018. Groundwater-surface water exchanges and associated nutrient fluxes in Dan'ao Estuary, Daya Bay, China. Continental Shelf Research, 166: 83–91, doi: 10.1016/j.csr.2018.06.014

Li Zhenyang, Pan Feng, Xiao Kai, et al. 2022. An integrated study of the spatiotemporal character, pollution assessment, and migration mechanism of heavy metals in the groundwater of a subtropical mangrove wetland. Journal of Hydrology, 612: 128251, doi: 10.1016/j.jhydrol.2022.128251

Li Hailong, Sun Pingping, Chen Shi, et al. 2010. A falling-head method for measuring intertidal sediment hydraulic conductivity. Groundwater, 48(2): 206–211, doi: 10.1111/j.1745-6584.2009.00638.x

Liu Yi, Jiao Jiujimmy, Cheng Hokwan. 2018a. Tracing submarine groundwater discharge flux in Tolo Harbor, Hong Kong (China). Hydrogeology Journal, 26(6): 1857–1873, doi: 10.1007/s10040-018-1736-z

Liu Yi, Liang Wenzhao, Jiao Jiujimmy. 2018b. Seasonality of nutrient flux and biogeochemistry in an intertidal aquifer. Journal of Geophysical Research: Oceans, 123(9): 6116–6135, doi: 10.1029/2018JC014197

Luo Manhua, Zhang Yan, Li Hailong, et al. 2022. Pollution assessment and sources of dissolved heavy metals in coastal water of

a highly urbanized coastal area: the role of groundwater discharge. Science of the Total Environment, 807: 151070, doi: 10.1016/j.scitotenv.2021.151070

Ma Qian, Li Hailong, Wang Xuejing, et al. 2015. Estimation of seawater–groundwater exchange rate: case study in a tidal flat with a large-scale seepage face (Laizhou Bay, China). Hydrogeology Journal, 23(2): 265–275, doi: 10.1007/s10040-014-1196-z

Mayfield K K, Eisenhauer A, Santiago Ramos D P, et al. 2021. Groundwater discharge impacts marine isotope budgets of Li, Mg, Ca, Sr, and Ba. Nature Communication, 12(1): 148, doi: 10.1038/s41467-020-20248-3

Millward G E, Liu Y P. 2003. Modelling metal desorption kinetics in estuaries. Science of the Total Environment, 314–316: 613–623

Montluçon D, Sañudo-Wilhelmy S A. 2001. Influence of net groundwater discharge on the chemical composition of a coastal environment: Flanders Bay, Long Island, New York. Environmental Science & Technology, 35(3): 480–486

Moore W S. 1999. The subterranean estuary: a reaction zone of ground water and sea water. Marine Chemistry, 65(1–2): 111–125

Moore W S. 2003. Sources and fluxes of submarine groundwater discharge delineated by radium isotopes. Biogeochemistry, 66(1–2): 75–93

Price R M, Swart P K, Fourqurean J W. 2006. Coastal groundwater discharge—an additional source of phosphorus for the oligotrophic wetlands of the Everglades. Hydrobiologia, 569(1): 23–36, doi: 10.1007/s10750-006-0120-5

Qu Wenjing, Li Hailong, Huang Hao, et al. 2017. Seawater-groundwater exchange and nutrients carried by submarine groundwater discharge in different types of wetlands at Jiaozhou Bay, China. Journal of Hydrology, 555: 185–197, doi: 10.1016/j.jhydrol.2017.10.014

Qu Shuyi, Wu Weihua, Nel W, et al. 2020. The behavior of metals/metalloids during natural weathering: a systematic study of the mono-lithological watersheds in the upper Pearl River Basin, China. Science of the Total Environment, 708: 134572, doi: 10.1016/j.scitotenv.2019.134572

Rengarajan R, Sarma V V S S. 2015. Submarine groundwater discharge and nutrient addition to the coastal zone of the Godavari Estuary. Marine Chemistry, 172: 57–69, doi: 10.1016/j.marchem.2015.03.008

Rodellas V, Garcia-Orellana J, Tovar-Sánchez A, et al. 2014. Submarine groundwater discharge as a source of nutrients and trace metals in a Mediterranean bay (Palma Beach, Balearic Islands). Marine Chemistry, 160: 56–66, doi: 10.1016/j.marchem.2014.01.007

Sanders C J, Santos I R, Barcellos R, et al. 2012. Elevated concentrations of dissolved Ba, Fe and Mn in a mangrove subterranean estuary: consequence of sea level rise?. Continental Shelf Research, 43: 86–94, doi: 10.1016/j.csr.2012.04.015

Santos I R S, Burnett W C, Chanton J, et al. 2008. Nutrient biogeochemistry in a Gulf of Mexico subterranean estuary and groundwater-derived fluxes to the coastal ocean. Limnology and Oceanography, 53(2): 705–718, doi: 10.4319/lo.2008.53.2.0705

Santos I R, Burnett W C, Dittmar T, et al. 2009. Tidal pumping drives nutrient and dissolved organic matter dynamics in a Gulf of Mexico subterranean estuary. Geochimica et Cosmochimica Acta, 73(5): 1325–1339, doi: 10.1016/j.gca.2008.11.029

Shum K T, Sundby B. 1996. Organic matter processing in continental shelf sediments—the subtidal pump revisited. Marine Chemistry, 53(1–2): 81–87

Sun Xia, Li Baoshi, Liu Xuanli, et al. 2020. Spatial variations and potential risks of heavy metals in seawater, sediments, and living organisms in Jiuzhen Bay, China. Journal of Chemistry, 2020: 7971294

Sun Zhigao, Mou Xiaojie, Tong Chuan, et al. 2015. Spatial variations and bioaccumulation of heavy metals in intertidal zone of the Yellow River Estuary, China. CATENA, 126: 43–52, doi: 10.1016/j.catena.2014.10.037

Syvitski J P M, Vörösmarty C J, Kettner A J, et al. 2005. Impact of humans on the flux of terrestrial sediment to the global coastal ocean. Science, 308(5720): 376–380, doi: 10.1126/science.1109454

Wang Xuejing, Li Hailong, Yang Jinzhong, et al. 2017. Nutrient inputs through submarine groundwater discharge in an embayment: a radon investigation in Daya Bay, China. Journal of Hydrology, 551: 784–792, doi: 10.1016/j.jhydrol.2017.02.036

Wang Qianqian, Li Hailong, Zhang Yan, et al. 2019. Evaluations of submarine groundwater discharge and associated heavy metal fluxes in Bohai Bay, China. Science of the Total Environment, 695: 133873, doi: 10.1016/j.scitotenv.2019.133873

Wang Qianqian, Li Hailong, Zhang Yan, et al. 2020. Submarine groundwater discharge and its implication for nutrient budgets in the western Bohai Bay, China. Journal of Environmental Radioactivity, 212: 106132, doi: 10.1016/j.jenvrad.2019.106132

Wang Xuejing, Li Hailong, Zheng Chunmiao, et al. 2018a. Submarine groundwater discharge as an important nutrient source influencing nutrient structure in coastal water of Daya Bay, China. Geochimica et Cosmochimica Acta, 225: 52–65, doi: 10.1016/j.gca.2018.01.029

Wang Xilong, Su Kaijun, Du Juan, et al. 2021a. Estimating submarine groundwater discharge at a subtropical river estuary along the Beibu Gulf, China. Acta Oceanologica Sinica, 40(9): 13–22, doi: 10.1007/s13131-021-1862-7

Wang Guizhi, Wang Shuling, Wang Zhangyong, et al. 2018b. Significance of submarine groundwater discharge in nutrient budgets in tropical Sanya Bay, China. Sustainability, 10(2): 380, doi: 10.3390/su10020380

Wang Qianqian, Wang Xuejing, Xiao Kai, et al. 2021b. Submarine groundwater discharge and associated nutrient fluxes in the Greater Bay Area, China revealed by radium and stable isotopes. Geoscience Frontiers, 12(5): 101223, doi: 10.1016/j.gsf.2021.101223

Wang Hua, Zhou Yiyi, Wang Xiao. 2016. Transport dynamics of Cr and Zn between deposited sediment and overlying water. CLEAN-Soil, Air, Water, 44(11): 1453–1460

Wen Xiaohu, Lu Jian, Wu Jun, et al. 2019. Influence of coastal groundwater salinization on the distribution and risks of heavy metals. Science of the Total Environment, 652: 267–277, doi: 10.1016/j.scitotenv.2018.10.250

Xiao Kai, Wu Jiapeng, Li Hailong, et al. 2018. Nitrogen fate in a subtropical mangrove swamp: potential association with seawater-groundwater exchange. Science of the Total Environment, 635: 586–597, doi: 10.1016/j.scitotenv.2018.04.143

Xu Bochao, Cardenas M B, Santos I R, et al. 2022. Closing the global Marine ^{226}Ra budget reveals the biological pump as a dominant removal flux in the upper ocean. Geophysical Research Letters, 49(12): e2022GL098087

Yin Xianqiang, Gao Bin, Ma L Q, et al. 2010. Colloid-facilitated Pb transport in two shooting-range soils in Florida. Journal of Hazardous Materials, 177(1–3): 620–625

Zhang Yan, Santos I R, Li Hailong, et al. 2020. Submarine groundwater discharge drives coastal water quality and nutrient budgets at small and large scales. Geochimica et Cosmochimica Acta, 290: 201–215, doi: 10.1016/j.gca.2020.08.026

Zhong Qiangqiang, Li Linwei, Puigcorbé V, et al. 2022. Contrasting behaviors of ^{210}Po, ^{210}Pb and ^{234}Th in the East China Sea during a severe red tide: enhanced scavenging and promoted fractionation. Acta Oceanologica Sinica, 41(8): 5–21, doi: 10.1007/s13131-021-1958-0